Check for updates

Original Article

Institution of MECHANICAL ENGINEERS
Journal of ENGINEERING IN MEDICINE

Proc IMechE Part H:
J Engineering in Medicine
2022, Vol. 236(12) 1720–1731
© IMechE 2022
Article reuse guidelines:
sagepub.com/journals-permissions
DOI: 10.1177/09544119221135687
journals.sagepub.com/home/pih
SAGE

The effect of friction stir process on the mechanical, tribological, and biocompatibility properties of AZ31B magnesium alloy as a biomaterial: A pilot study

Hojjat Ghahramanzadeh Asl[1], Selcen Celik-Uzuner[2], Ugur Uzuner[2], Yaşar Sert[1] and Tevfik Küçükömeroğlu[1]

Abstract

Recently, AZ31B magnesium alloy has been widely employed in automotive, aerospace, and bio implant industries due to its light-weight and biocompatibility properties. However, the equilibrium of ductility and strength of this material and the negativity brought by its poor wear behavior have limited its versatile use. Friction stir processing (FSP) has been commonly used as severe plastic deformation method for improving mechanical and tribological properties of metal sheets. The effect of this method on the biocompatibility of materials is a matter of curiosity that should be emphasized. So, the present study aims to investigate the effect of friction stir process on the mechanical, tribological, and biocompatibility properties of AZ31B magnesium alloy. It is observed that FSP enhanced the tensile properties of the alloy but decreased its elongation. It was determined that the base material exhibited ductile character on the fracture surface of the specimens, and mixed ductile/brittle fracture was evident with the FSP. In the FSP zone, the hardness value was improved by 17% compared to the base material. Also, the wear performance of the alloy enhanced in ambient air and Simulated Body Fluid (SBF) solution. Wear properties in SBF solution were better due to less adhesive bonds between the friction surfaces. This assessment was supported by SEM images of the wear path and surface of counter bodies. On the other hand, FSPed AZ31B alloy materials with improved strength properties were not cytotoxic for human gingival fibroblasts, and these results may suggest that the materials are safe for clinical uses.

Keywords

AZ31B, FSP, tensile strength, wear, cytotoxicity

Date received: 7 May 2022; accepted: 10 October 2022

Introduction

Magnesium alloys such as AZ31B have the advantages of high specific strength and low density, and thus they are commonly used in transportation, electronics, automotive, and aerospace industries.[1,2] Besides, biodegradable magnesium and its alloys are quite suitable for bio implant application due to the biocompatibility, similar elastic modules to human bone, and their nontoxic oxide properties.[3] The standard value for biocompatibility is expected as at least 70% of cell viability.[4] Despite the desirable properties, these alloys have restricted slip systems because of their hexagonal closed packed structure. Thus, their usage area is substantially limited due to the tribological properties.[5] In addition to this limitation, the ductility and strength equilibrium of AZ31B alloys is still undesired feature by their coarse grained structure.[6]

In mechanical parts, the grain size is regarded as an important factor for its mechanical and tribological behavior. The grain refinement is achieved employing severe plastic deformation (SPD) techniques.[7] It is

[1]Department of Mechanical Engineering, Faculty of Engineering, Karadeniz Technical University, Trabzon, Turkey
[2]Department of Molecular Biology and Genetics, Faculty of Science, Karadeniz Technical University, Trabzon, Turkey

Corresponding author:
Hojjat Ghahramanzadeh Asl, Department of Mechanical Engineering, Faculty of Engineering, Karadeniz Technical University, Ortahisar/Trabzon 61080, Turkey.
Email: h.kahramanzade@ktu.edu.tr

emphasized in the literature that using the SPD, conspicuous improvement in the strength of magnesium alloys are obtained.[8,9] Among these SPD techniques, high pressure torsion (HPT), multi-axis forging, and equal-channel angular pressing (ECAP) are frequently employed.[10] However, the SPD techniques mentioned above are only suitable for bulk materials, not for sheet metals, especially in the localized regions. Additionally, these methods are not feasible because they are very complex, time consuming, and also have high initial costs.[7] To overcome these disadvantages, a technique derived from Friction Stir Welding (FSW) and called as Friction Stir Process (FSP) has been developed.[11] In recent years, FSP has gained attention as a solid-state material processing technology that improves mechanical properties by altering the microstructure of mechanical parts.[12] In this technique, a rotating tool, be composed of a probe and a shoulder, immersions into the plate and moves with traversal speeds and constant rotational in the ambitioned direction. Also, the plate is moved around the tool from front to back. Previously, FSP technology has been extensively studied to enhance the mechanical properties of titanium alloys,[13,14] copper alloys,[15,16] aluminum alloys,[17,18] and steel.[19,20] Apart from these materials, limited study has been performed on FSP of magnesium alloys. In one of them, the effect of FSP on microstructure of AZ91 magnesium alloy is investigated, and achieved homogenization and grain refinement of the untreated alloy.[21] The effects of FSP on the formability and mechanical features of Mg AZ31B alloy were previously examined in another work (Venkateswarlu et al.[22]). A remarkable improvement in the mechanical properties and formability is determined owing to more homogenization of the base material.[22] Besides, various studies have been performed in the literature on the biocompatibility of magnesium alloys.[23]

AZ31B alloys stand as new generation of biodegradable and bioresorbable metallic materials for consumable bio implant applications owing to their good biocompatibility and high similarity to the mechanical properties of human bone.[24,25] In addition, Mg ion is the fourth most abundant and needed cation in the human body and highly essential to promote bone cells activation and proliferation.[2] It also favors strength, mineralization, and growth of bone,[26] through osteointegration. Mg is also essential for the biosynthesis and genetic stability of nucleic acid materials and serves as a stabilizer on DNA and RNA structures by interacting with phosphate groups as counter ions thereby neutralizing the negative charges.[27,28]

Mg alloys exhibit bone-like physico-chemical and biological properties, which are essential requirements for implant materials.[29] As Mg implants are biodegradable and gradually decompose in the body environment, they are more suitable materials for short-term implants, excluding the need for secondary surgical interventions.[30] Nevertheless, high degradation rate of Mg alloys in the physiological environment limits their suitability for long-term clinical applications.[31] Such degradation locally increases alkalization and free Mg ions, eventually reducing the in vivo integration rate between the tissue and Mg implant.[32] However, surface modification techniques have provided favorable conditions to control the degradation rate of Mg alloys and increase surface biocompatibility without changing bulk properties. Therefore, the selection of Mg implant resurfacing processes and materials that impart corrosion resistance and stimulate the biological response of the living tissue surrounding the implants has gained great importance.

The present study thus aimed to examine the effect of FSP on the improvement of mechanical and wear properties of AZ31B alloy as well as monitoring the cytotoxicity of the modified alloy. This study is considered as a pilot study and as a result of the satisfactory findings given in results and discussion section, it is planned to carry out the optimization studies for the FSP on AZ31B alloys in future studies. In this context, the mechanical evaluation consisting of micro-hardness testing, tensile testing, and fractography was performed. Furthermore, ball-on-disc type tribotester was used to investigate the tribological features of the base material and FSPed alloy under ambient air and simulated body fluid (SBF) solution. In addition, the wear rate on the surfaces in both environments was determined by optical profilometer. The wear mechanisms of the materials were investigated as a result of SEM and EDS analysis. In addition, the biocompatibility of both the base material and FSPed AZ31B alloy implant biomaterials were determined by cell biocompatibility tests performed by MTT test to understand whether the base material and FSPed specimens have cytotoxicity properties for human cells.

Material and method

Material and process

AZ31B alloy plates (Al ~3, Zn ~ 0.8, Mn ~ 0.2, Si ~ 0.1, and bal. Mg)[22] having dimensions of $100 \times 25 \times 5$ mm^3 was used as base material in this study. AZ31B plates subjected to the Friction Stir Process (FSP) were fixed by the shoes on the upper table of the hydraulic assembly given in Figure 1. In this hydraulic loading mechanism, there are hydraulic pistons and four guide shafts placed on the fixed lower table. The movable upper table, which is mounted on the guide shafts, can be moved in the direction of the tool axis owing to the hydraulic piston. In order to keep the tool pressure balanced in every part of the table, four opposing springs were placed on the movable table. The advance direction of the AZ31B alloy plates was vertical to the FSP direction. FSP process was performed on the base material using a specified tool with a rotational speed of 45 mm$\times$min^{-1}, traversing at 1000 rpm, and pressure force of 5 kN. The tilt angle of FSP tool was kept

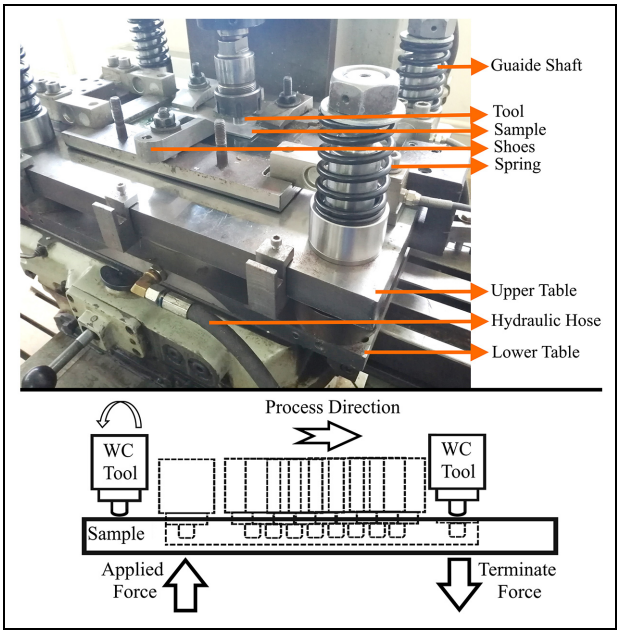


Figure 1. Detail view and application schematic of the friction stir process setup.

constant at 2°. FSP was performed using A tungsten carbide (WC) tool consisted of a shoulder with the diameter of 18 mm and the 30° cone angle. The WC tool with 18 mm diameter used in FSP is illustrated in Figure 2(a). In addition, the temperature of the AZ31B alloy was controlled and kept between 40°C and 60°C by cooling during FSP. After FSP treatment, specimens were chemically etched with natal 10 pct for microstructure evaluations.[33]

Mechanical and tribological tests

After the FSP was performed, the specimens were taken from the process areas of the AZ31B plate to investigate the mechanical and tribological properties as shown in Figure 2(b).

Hardness values of the base material and the specimens obtained from FSPed zone were determined using Vickers micro-hardness tester (Struers Duramin 3, Denmark) under 10 gr constant load and 10 s dwell time.

The tension test samples were taken from the FSPed zone parallel to the process direction by wire-electron discharge machine (EDM). Tensile tests were performed using the shape of a dog-bone sample which in accordance with the ASTM E8 with dimensions shown in Figure 2(c). The tests were performed employing a tensile tester (Instron-3382, USA) at 1×10^{-3} s^{-1} strain rate. The fracture surfaces of the tensile specimens were investigated using SEM (Zeiss EVO LS10, Germany).

The tribological tests were carried out using DUCOM (TR-201, India) ball-on disc tribometer under the condition of ambient air and in simulated body fluid (SBF).[34] The ion concentration of SBF is shown in Table 1. The sliding speed was set as 100 rpm with the diameter of 8 mm and the sliding distance was ~25.12 m and the applied constant normal load was 1 N. The topography of wear path and volume of wear were determined by an optical profilometer (NANOFOCUS, μscan Custom, Germany). The wear rates of the samples were calculated using the Archard formula (1).

$$W = V/(P * d) \quad (1)$$

In related formula, W, V, P, and d is stated the wear rate (mm^3/N.m), wear volume (mm^3), applied constant normal load (N), and distance of sliding (m), respectively. SEM investigation was carried out to determine the main wear mechanisms of friction surfaces. Also, map-EDS examination was carried out from worn surface and specimens' surface for chemical analyses.

Cell culture, MTT assay and statistical analyses

EN ISO 10993–5 was used as a standard for MTT assay to analyze cytotoxicity. Before MTT assay, human gingival fibroblast (hGF) (ATCC, PCS-201-018™) cells were cultured in DMEM media including 10% fetal bovine serum and %1 Penicillin-Streptomycin at 37°C incubator with 5% CO_2 humidification. Cells were initially seeded into 96-well plates.

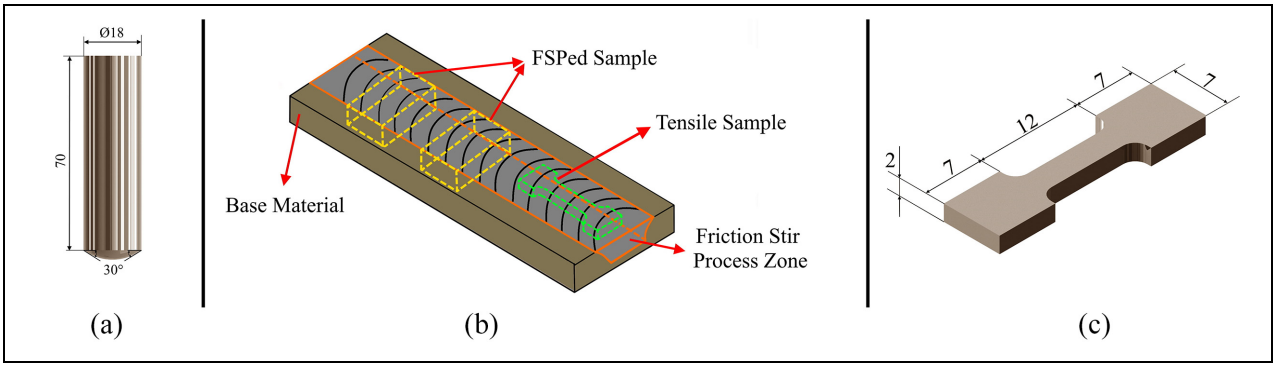


Figure 2. The schematic of the geometry of tool used in friction stir process (a), location of test samples taken from the FSPed plate (b), and the tensile test specimen dimensions (c).

Table 1. Ion concentrations of SBF.[34]

	Na^+	$K+$	Mg^{2+}	Ca^{2+}	HCO^-_3	HPO_4^{2-}	pH
SBF	142.0	5.0	1.5	2.5	4.2	1.0	7.4

After they reached 80% confluency, base material and FSPed AZ31B alloy specimens were dipped into the wells, each three of wells was incubated with materials for 24, 48, and 72 h. Control cells were not incubated any of materials, but media only was refreshed. After incubations, base material and FSPed AZ31B were removed carefully, cells were proceeded with MTT protocol for cytotoxicity. MTT (3-(4,5-Dimethylthiazol-2-yl)-2,5-Diphenyltetrazolium Bromide) is a yellowish soluble tetrazolium salt and this is used for colorimetric analysis to detect cell viability through redox potential of the cells. MTT is converted by viable cells so that these cells convert yellow to blue-purple, however dead cells cannot use MTT resulting in persistent yellowish appearance.[35] MTT protocol briefly was applied as follows: (1) media removal after taking out the materials, (2) washing wells with 1xPhosphate-Saline Buffer (PBS) for two times, (3) 190 µl of media and 10 µl of MTT addition to each well followed by the incubation for 2 h at 37°C, (4) removal of media including MTT followed by 200 µl of dimethylsulfoxide addition to each well and incubation at room temperature overnight in the dark and on shaker, and (5) The day after cells were spectrophotometrically read at 570 nm using a microplate reader, as previously performed.[36] Viable cells are supposed to have higher absorbances as possible, and the absorbance differences between treated and untreated cells conclude if the application of materials is cytotoxic or not. Absorbances were then statistically analyzed by SPSS software (Version 23) using Post-hoc of UNIANOVA test (univariate analysis of variance) for pair comparisons. Significance levels used were $p < 0.05$(*), $p < 0.01$(**), $p < 0.001$ (***) and $p < 0.0001$(****).

Results and discussion

Microstructure analyses

Figure 3 shows the microstructure of FSP treated and untreated zone of the AZ31B alloy. As can be seen in this figure, the grain structure of the AZ31B alloy can be clearly seen in the untreated region. However, the flow direction under tension in the material is clearly visible, in the FSP treated region. It is seen from the positions of the flow lines that these flows occur in a very narrow range. It is known that the grain structure becomes too thin to be visualized in an optical microscope with the high tension applied in such a narrow area. Therefore, grain refinement in the structure is revealed by XRD analysis which is given in Figure 4. According to the analysis of X'Pert Software, the FWHM (Full Width at Half Maximum) of the peaks are broadened. It is known that the increase in the widths (FWHM) values of the peaks obtained in the materials is a sign that the grain size decreases.[37] Ge and Xiang have observed similar results.[5] In addition, it was determined that the secondary phase provided by the precipitated Mg17Al12 structure was formed in the structure after the FSP treatment.[5] Apart from this phase, other phases are formed in the same α-Mg structure in both specimens.

Mechanical properties

Figure 5 presents the micro-hardness values of base material and FSPed AZ31B alloy. As seen, FSP enhanced the micro-hardness of the base material from 65 $HV_{0.01}$ to 76 $HV_{0.01}$. This improvement on the hardness value is attributed to complex material flow and extreme plastic deformation phenomena.[38] The increase in dislocation density and grain refinement by the reason of the extreme plastic deformation on the alloy surface with FSP improved the hardness, approximately ~17%. According to the literature, one of the main reason for the increase is the strengthening of the

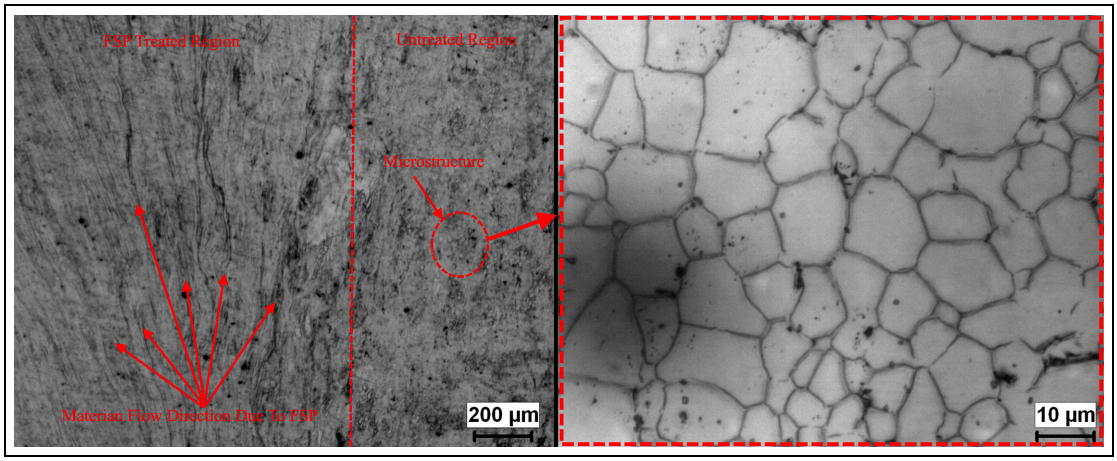


Figure 3. Optical microscope image of FSP treated and untreated zone of AZ31B alloy.

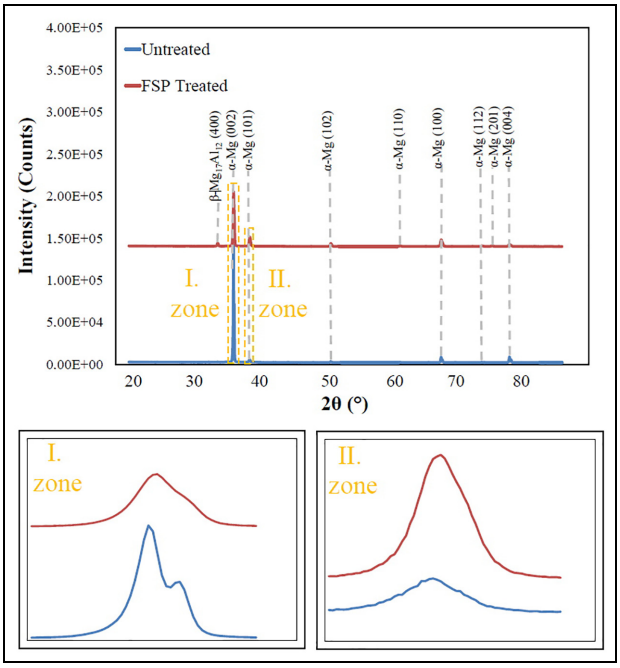


Figure 4. XRD graph of the FSP treated and untreated zone of AZ31B alloy.

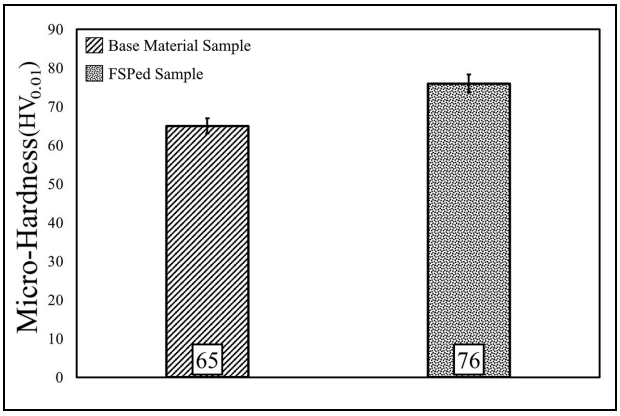


Figure 5. Micro-hardness values of specimens untreated and FSPed AZ31B alloy.

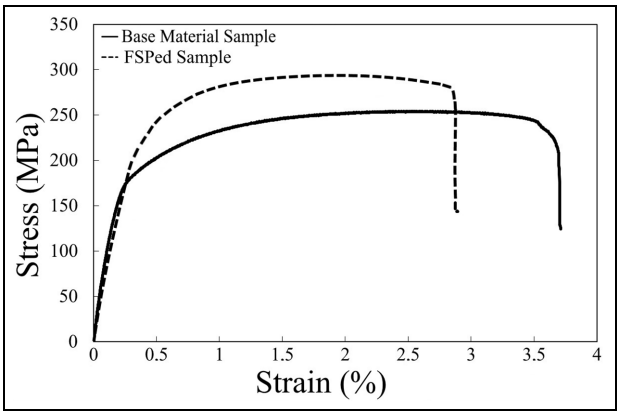


Figure 6. Strain-Stress curves of the base material and FSPed alloy.

second phase provided by the $Mg_{17}Al_{12}$ structure which is shown in Figure 4 precipitated in the processed zone.[5]

Figure 6 presents the stress-strain curves of the base material and FSPed alloy. As Figure 6, the yield and tensile strength of the AZ31B alloy is enhanced in the FSP zone compared to the base material.

As seen in Figure 6, while the maximum tensile strength value is 253.6 MPa for the base material, this value reaches 291.8 MPa for the FSPed alloy. This shows that ~16% increase in tensile strength is achieved.

The considerable situation here is that the amount of increase is close to the amount of increase in hardness strength.[39] Owing to the FSP, the effect of the second phase and grain boundary strengthening mechanisms mentioned above becomes more evident due to the reduced basal tissue density on the surface, and it contributes to the enhancement of the yield strength.[40] The reduction in tensile ductility seen in the FSPed specimen compared to the base material is related to the strain hardening properties. In the literature, the decrease in the hardenability of strain in the FSPed specimen is attributed to the enhanced the density of dislocation.[41] It is clearly known that the primary hardening mechanism of polycrystalline materials is that microstructural barriers and other dislocations in the internal structure prevent the dislocation movement.[42] It is seen that the level of decrease in the deformation ability of the FSPed alloy is at an acceptable level according to the studies in the literature.[43]

The fracture surface of the tensile-tested specimens is given in Figure 7. As seen in Figure 7(a), the base material exhibits a large number of dimples indicating the ductile fracture. On the contrary, the FSPed specimen (Figure 7(b)) presents both dimples and cleavage facets. For the FSPed alloy, some dimples contain precipitates, which expresses mixed ductile/brittle fracture. Besides, the river patterns are observed for the FSPed alloy' fractured surface. This pattern is presented the more cleavage brittle fracture properties compare to base material. SEM images of the fracture surfaces of the specimens are in accordance with the findings of the tensile test.

Tribological properties

The coefficient of friction (CoF) curves of the specimens under dry sliding (ambient air condition) and in SBF are illustrated in Figure 8. Under both conditions, the FSPed alloy exhibits lower CoF values compared

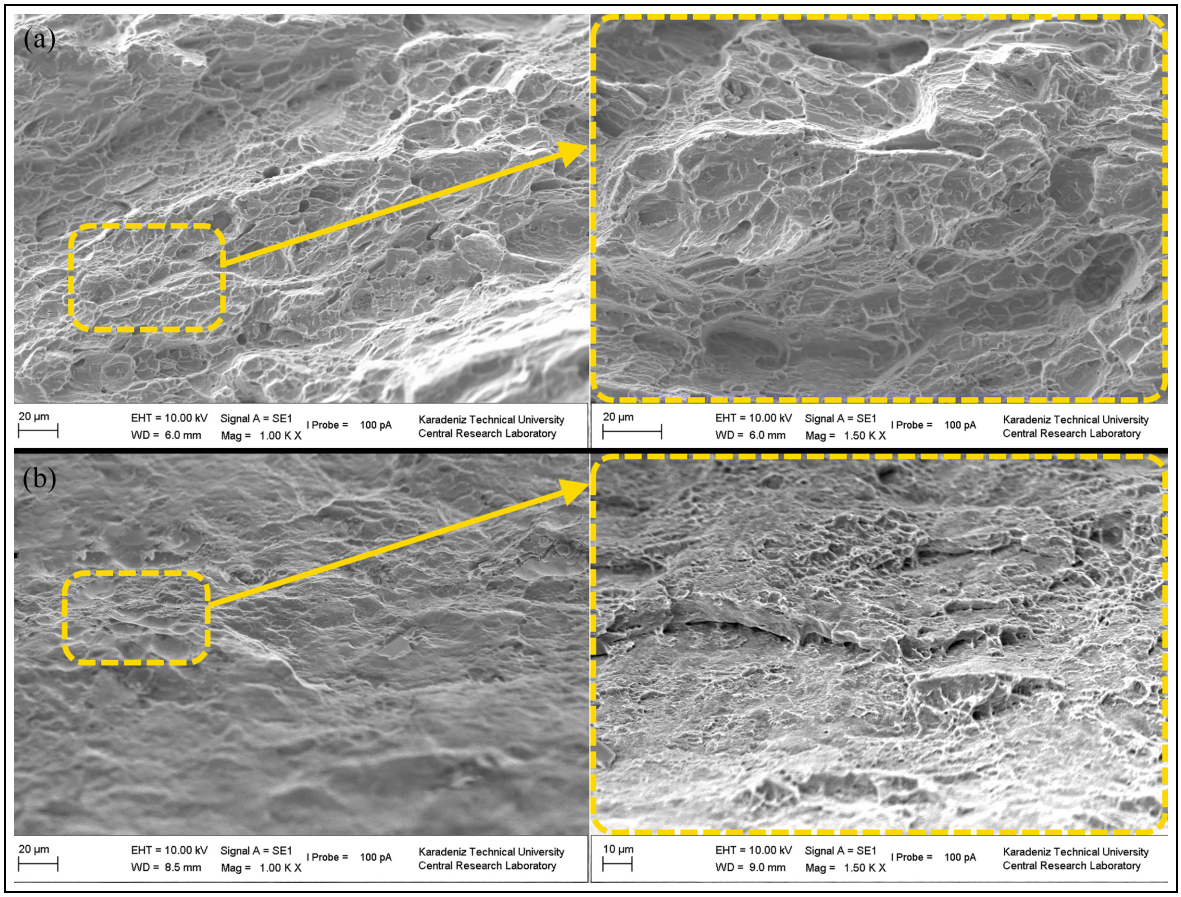


Figure 7. SEM fractographs of the (a) base material, and (b) FSPed specimens after the tensile test.

to the base material. In addition, the CoF values of the specimens are lower in the wear tests carried out in SBF solution. It is seen that the fluctuations in the CoF curve of the materials in the ambient air conditions are high intensity and frequency. In the tribological tests carried out in SBF solution, the graphic fluctuations of the materials are more stable and regular than in other condition. This is attributed to the adhesive contact between the AZ31B alloy and the counter body surface.[44] Similar results were obtained with the studies carried out in the SBF environment in the literature.[45] The friction coefficient graphs were more fluctuant due to the accumulation of oxide particles on the surface Huang et al. indicated that in the presence of the SBF, the CoF fluctuations are more stable than air in the wear tests.[45] In the tribological tests performed in the SBF solution, the particles move away from the contact area with the effect of centrifugal force. Owing to the FSP, the CoF decreased due to the homogeneous distribution and fine microstructure formed on the alloy surface.[46] In addition, the increase in hardness and plastic deformation strength can be shown as the reason for the decrease in CoF value.

The optical profilometer illustrations of wear paths under ambient air and in SBF solution are shown in Figure 9. According to Figure 9, the depth and of the wear path are more explicit and larger than other

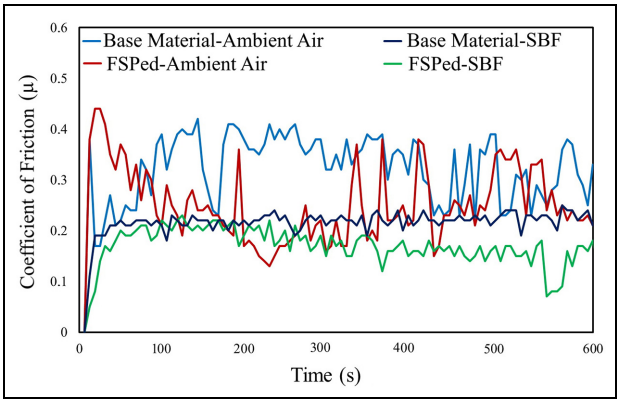


Figure 8. The CoF graphs of specimens tested under ambient air and SBF conditions.

condition in the tribological tests carried out under ambient air. However, as seen in Figure 9 (Figure 9(c) and (d)), the wear performance of FSPed specimens is higher than in the base material (Figure 9(a) and (b)). The wear rate values obtained as a result of optical profilometer examinations are shown in Figure 10. According to the relevant figure, it is observed that the wear performance of the AZ31B alloy is improved applying the FSP. This said increase is ~14% in both environments. This observed increase is associated with

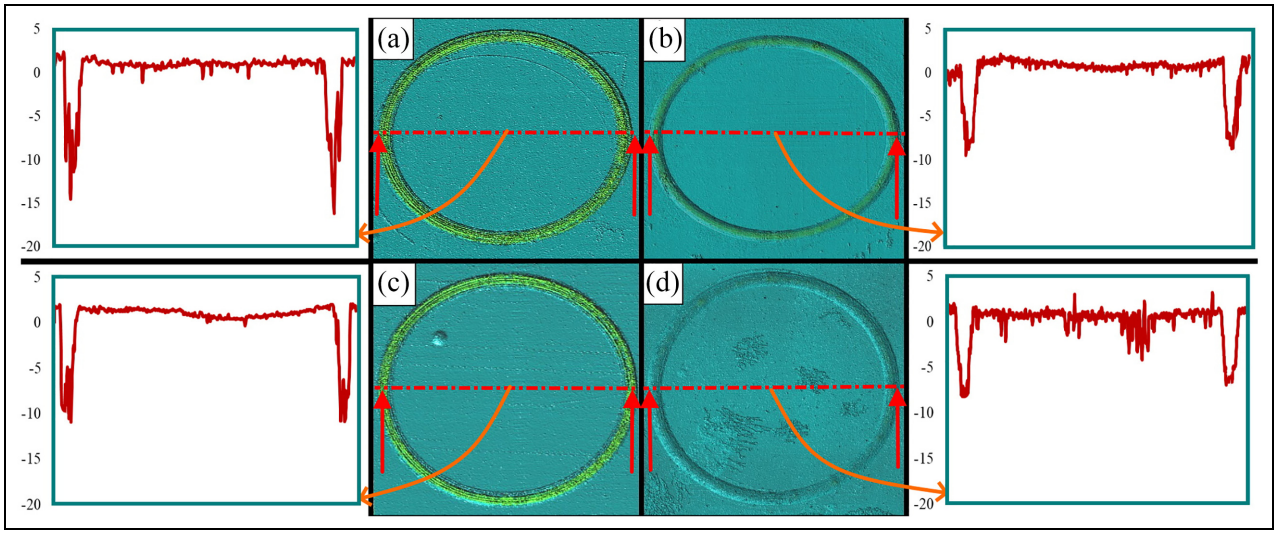


Figure 9. The optical profilometer image of worn path of specimens: (a) base material-ambient air, (b) base material-SBF, (c) FSPed-ambient air, and (d) FSPed-SBF.

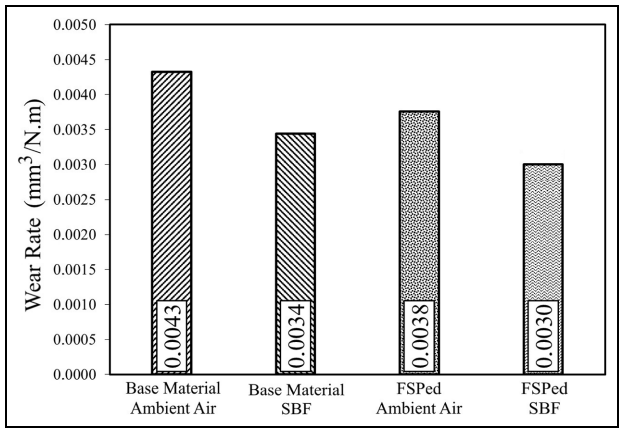


Figure 10. The wear rate of specimens: (a) base material-ambient air, (b) base material-SBF, (c) FSPed-ambient air, and (d) FSPed-SBF.

the homogenization of the alloy microstructure and its improved resistance to plastic deformation owing to the FSP.[47] Archard's law of wear states that hardness and rate of wear are inversely proportional as seen in Figures 5 and 10. In addition, it is seen that the wear rate is lower in the tests carried out in SBF. In both base material and FSPed alloy, the wear rate value in the SBF solution medium is ~26% less than in ambient air. The reason for this is the rapid cooling of the micro welds formed due to the adhesive characteristic.[45] Thus, the dominant wear mechanism turned into the adhesive wear to plastic deformation in SBF solution.

Table 2 shows the chemical composition obtained from the surfaces and detailed worn surfaces of the specimens. It is observed that there is a higher amount of oxygen on the surface of the FSPed alloy compared to the base material. This situation is caused by oxidations that occur with temperature during the FSP.[48] Besides, the Zn ratio in the FSPed AZ31B alloy is higher than the untreated alloy (1.3%), with a value of 2.4%. For the case of FSPed alloy, obtained percentage of Zn ratio of 2.4 is suitable with the literature.[49] According to the table, it is seen that the amount of oxygen in the wear trace (6.8%) increased in the wear test carried out under ambient air condition on the base material. In the FSPed specimen, the amount of oxygen caused by friction heat in the ambient air condition increased up to 14%. This increase in oxygen is less in the SBF solution. While the oxygen content is 7.3% in the SBF solution on the base material wear path, this value is 9.2% for the FSPed alloy. This situation is attributed to the low level of oxidation on the surface due to rapid cooling of the friction heat in the wear tests performed in the SBF solution and the hasty rupture of micro-welding.[50]

Figure 11 presents the SEM images of the wear paths of base material and FSPed alloy under both conditions. These SEM investigations provide a deeper conception of the effect of FSP on wear features. The wear mechanism of the base material in ambient air is the consist of larger scratches, wrinkles, and delamination which indicated the adhesive wear characteristics (Figure 11(a)).[51] The scratches on the surface are formed as a result of the wear particles getting stuck between the mating surfaces due to the breaking of the micro weld connections formed in the said adhesive characteristic.[52] It is observed that the worn surface of the base material in SBF solution (Figure 11(b)) has smoother and shallower scratches compared to the ambient air. This is because of the micro-welding joints break relatively easily and early due to the rapid cooling of the frictional heat between the mating surfaces in the SBF solution.[45] In the detail view enclosed in the yellow

Table 2. Chemical composition of specimens' worn surfaces under ambient air and SBF conditions (wt%).

	Mg	Al	Zn	O
Base Material Surface	90.4	3.5	1.3	4.8
Base Material Worn Surface Ambient Air	88.9	3.3	1.0	6.8
Base Material Worn Surface SBF	87.5	3.9	1.3	7.3
FSPed Surface	85.1	3.6	2.4	8.9
FSPed Worn Surface Ambient Air	79.8	3.6	2.4	14.2
FSPed Worn Surface SBF	87.2	3.2	0.4	9.2

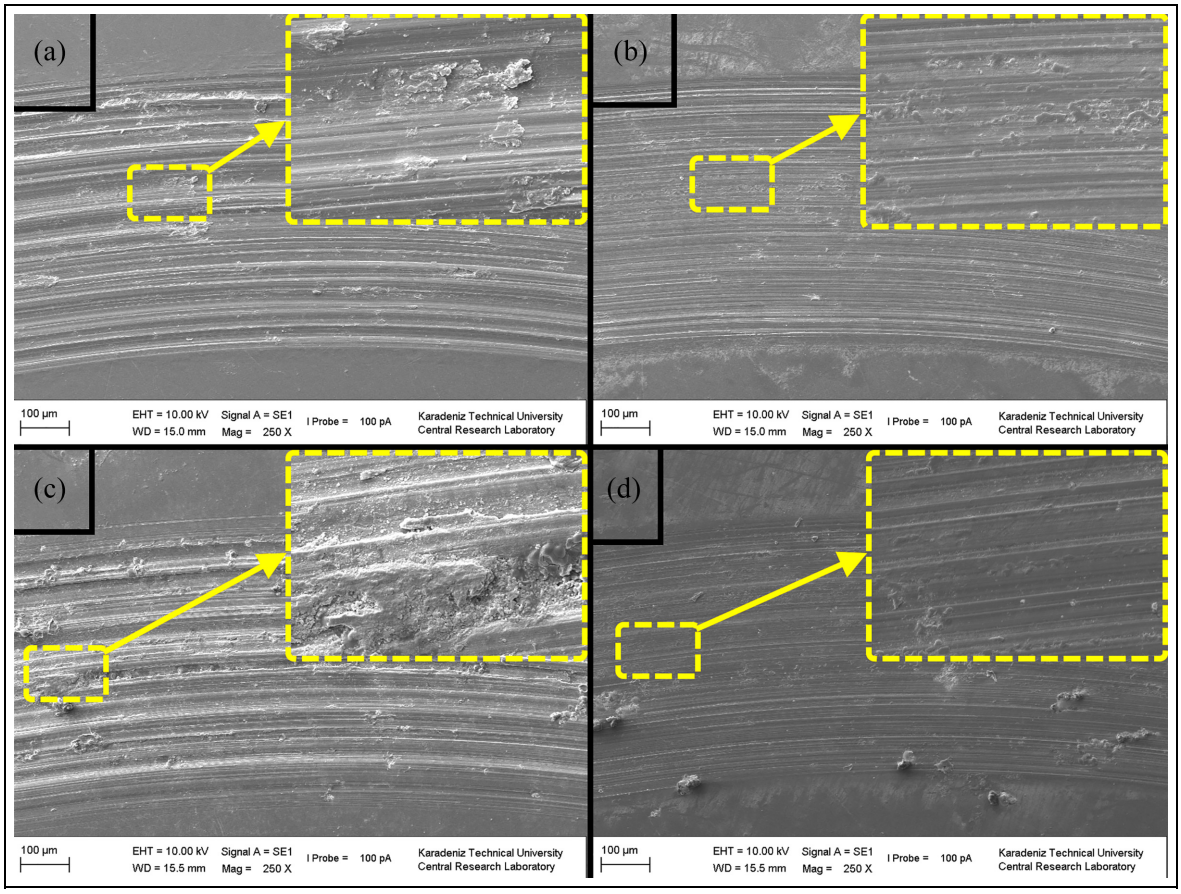


Figure 11. SEM images of worn surfaces of specimens: (a) base material-ambient air, (b) base material-SBF, (c) FSPed- ambient air, and (d) FSPed-SBF.

box, it is seen that the weld joints are present and that it is insipid compared to the experiments carried out in ambient air. However, the presence of wear debris is also few and far between, compared to Figure 11(a). It is possible that the wear debris are separated from the wear path by dispersing into the SBF solution with the effect of the rotating speed. Although the wear path of the FSPed alloy in ambient air (Figure 11(c)) exhibits a similar wear characteristic with the base material, the breaking of the adhesive bonds seen in detail view has become difficult owing to the higher plastic deformation strength. However, even with high hardness, abrasive scratches appear to be present. Compared to the base material, less deep scratches occur, that is confirming Figure 10. The difference between the wear path of the FSPed alloy in the SBF solution and the ambient air is shown in Figure 11(d). Unbroken adhesive bonds and prominent abrasive scratches in Figure 11(c) are almost non-existent here. It has a very smooth and superficial wear path compared to the base material in Figure 11(b). This observed situation is in full agreement with the wear rate values given in Figure 10.

Figure 12 presents the surfaces of the counter body under both wear test conditions. These images support the statements of the wear characteristic in all specimens. It is seen that the base material and FSPed alloy are plastered on the counter body surface under the ambient air (a and c). It is seen that more distinct plastering occurs on the counter body of the base material. This situation can be explained by the decrease in

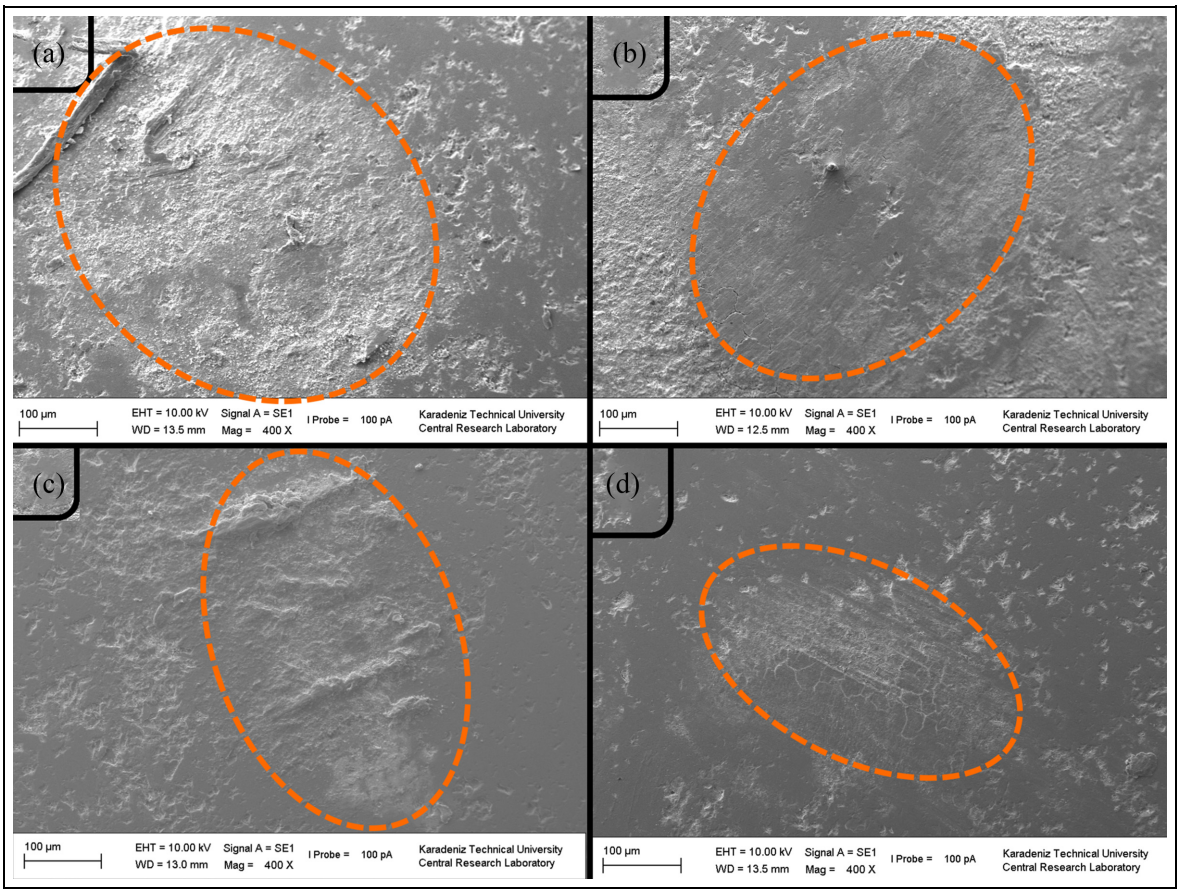


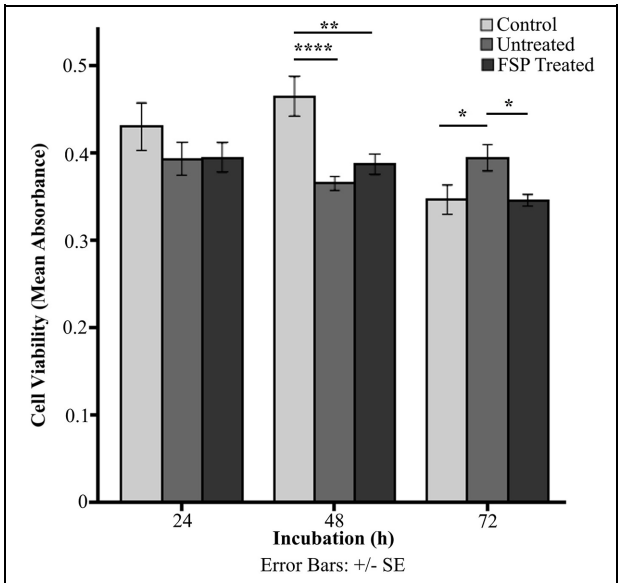
Figure 12. SEM images of counter body surface under both conditions: (a) base material-ambient air, (b) base material-SBF, (c) FSPed- ambient air, and (d) FSPed-SBF.

plastic deformation ability as a result of applied FSP.[43] It is noted that in the SBF solution, the plastered region on the counter body surface are relatively lower in the both of specimens compare to ambiet air condition. This is attributed to the absence of micro-welds between the friction surfaces in the SBF solution or the lesser level of plastering due to rapid cooling. Besides, It is observed that the trace size formed on the counter body of the base material is more pronounced than the FSed alloy. This situation supports the wear rate values seen in Figure 10.

Cytotoxicity analyses

The biocompatibility of implant biomaterials is critical, and thus the cell biocompatibility on base material and FSPed AZ31B alloy was evaluated by MTT assay. hGF cells were treated with base material and FSPed AZ31B alloy specimens as mentioned in the materials-methods section. It was identified that the cell viability was not affected by any material at the first 24 h incubation ($p > 0.05$). When the base material and FSPed AZ31B alloy specimens were incubated with cells for 48 h, however, a significant decrease in cell viability ($p < 0.05$) for both untreated and FSP treated materials was observed. Yet for longer incubation periods (72 h), the cells treated with any material were quite viable in number compared to control cells (Figure 13). Moreover, even untreated material was able to induce a higher cell viability rate during the incubation with gingival fibroblast cells. These results indicated that FSPed AZ31B alloy materials with improved strength properties do not induce cytotoxicity in human gingival fibroblasts, suggesting that candidate materials are safely applicable for biological uses in human body. The current results thus confirmed the biocompatibility of FSPed AZ31B alloys.

Although previous studies reported that Mg alloys reveal moderate cytotoxic effects on CHO-K1 cells due to the rapid release of biocorrosion products,[53] recent surface modification studies further improved the biocompatibility and degradation resistance of AZ31B alloys.[32] Unlike polymeric and ceramic biomaterials, Mg alloys present a new arsenal to dentistry, implantation and peripheral nerve regeneration approaches due to their biodegradable and superior lightweight mechanical properties.[54,55] The density and elastic modulus values of AZ31B Mg alloys are much akin to human bone, particularly minimizing stress shielding and associated effects For instance, Rajan et al. recently modified the surface of AZ31B alloys with thin niobium oxide films to overcome high degradation and



Comparisons		Significance		
		24h	48h	72h
Control	Untreated	n.s	$p<0.0001$	$p<0.05$
Control	FSP Treated	n.s	$p<0.01$	n.s
Untreated	FSP Treated	n.s	n.s	$p<0.05$

n.s: not significant

Figure 13. Cell viability after treated and untreated materials at 24, 48, and 72 h with statistical comparisons between applications.

corrosion rates, which eventually improved overall corrosion resistance, hemocompatibility, biocompatibility and cell proliferation of AZ31B Mg alloys.[56] Taken together, surface-modified AZ31B alloys stand as biocompatible implant biomaterials for orthopedic implants and regenerative medicine applications.

Conclusions and future works

In this pilot study, an attempt was performed to investigate the effect of FSP on the mechanical, tribological, and biocompatibility properties of AZ31B magnesium alloy. The FSP was successfully applied to the AZ31B alloy with the specified tool tip, process parameters, and cold source assistant. Upon FSP treatment, the tensile strength and hardness of the alloy have improved by ~16% due to the second phase strengthening mechanism, while its ductility has reasonably decreased. The fracture surfaces of the samples shed light on the evaluation of mechanical properties. In other words, while the fracture surface of the FSPed alloy was mixed ductile/brittle characteristic, the base material exhibited ductile fracture. In addition, under dry sliding and in SBF solution, FSP improved the poor wear behavior of the AZ31B alloy by 14%, and 26%, respectively. During the wear tests performed in the SBF solution, the absence of adhesive wear (micro-weld joints) had a positive effect on the wear properties. On the other hand, FSP AZ31B alloys with improved strength properties did not induce cytotoxicity in human gingival fibroblasts, suggesting thatFSP AZ31B alloys can be considered as safely applicable candidate materials for versatile use such as dental applications.

As a result of this pilot study, it has been proven that the improvability of mechanical and wear performance without adversely affecting the cytotoxicity of AZ31B alloy by FSP. In future studies, the wear performance of the AZ31B alloy can be optimized by changing both the FSP parameters and the tool geometry. Before in vivo studies, the effect of FSP on osteoblast and mesenchymal stem cells is an open subject to investigate. In addition to cytotoxicity, more extensive preclinical testing for their use in the human body, including biological analysis and in vivo studies, remains unclear as further studies.

Acknowledgement

We thank to Dr Hatice SEVIM NALKIRAN (Recep Tayyip Erdogan University, Department of Medical Biology, Rize - TURKEY) for providing a batch of primary human gingival fibroblast cells.

Declaration of conflicting interests

The author(s) declared no potential conflicts of interest with respect to the research, authorship, and/or publication of this article.

Funding

The author(s) received no financial support for the research, authorship, and/or publication of this article.

ORCID iDs

Hojjat Ghahramanzadeh Asl https://orcid.org/0000-0002-9078-1933
Yaşar Sert https://orcid.org/0000-0001-7742-0335

References

1. Mao B, Liao Y and Li B. Gradient twinning microstructure generated by laser shock peening in an AZ31B magnesium alloy. *Appl Surf Sci* 2018; 457: 342–351.
2. Mordike BL and Ebert T. Magnesium: properties-applications-potential. *Mater Sci Eng A* 2001; 302: 37–45.
3. Sunil BR, Kumar AA, Sampath Kumar TS, et al. Role of biomineralization on the degradation of fine grained AZ31 magnesium alloy processed by groove pressing. *Mater Sci Eng: C* 2013; 33: 1607–1615.
4. Comba A, Cicek B, Comba B, et al. Investigation of in-vitro biocompatibility and in-vivo biodegradability of AM series Mg alloys. *Mater Technol* 2022; 1–13. DOI: 10.1080/10667857.2022.2081115.

5. Ge M-Z and Xiang J-Y. Effect of laser shock peening on microstructure and fatigue crack growth rate of AZ31B magnesium alloy. *J Alloys Comp* 2016; 680: 544–552.
6. Xu N, Song Q, Bao Y, et al. Investigation on microstructure and mechanical properties of cold source assistant friction stir processed AZ31B magnesium alloy. *Mater Sci Eng A* 2019; 761: 138027.
7. Ramesh Babu S, Senthil Kumar VS, Karunamoorthy L, et al. Investigation on the effect of friction stir processing on the superplastic forming of AZ31B alloy. *Mater Des* 2014; 53: 338–348.
8. Estrin Y and Vinogradov A. Extreme grain refinement by severe plastic deformation: A wealth of challenging science. *Acta Mater* 2013; 61: 782–817.
9. Chang S-Y, Lee S-W, Kang KM, et al. Improvement of mechanical characteristics in severely plastic-deformed Mg Alloys. *Mater Trans* 2004; 45: 488–492.
10. Karthikeyan L, Senthilkumar VS and Padmanabhan KA. Biaxial stressing of sheets of friction stir processed aluminum alloy A319. *Mater Manuf Process* 2010; 25: 1297–1303.
11. Mishra RS and Ma ZY. Friction stir welding and processing. *Mater Sci Eng R Rep* 2005; 50: 1–78.
12. Patel V, Li W, Andersson J, et al. Enhancing grain refinement and corrosion behavior in AZ31B magnesium alloy via stationary shoulder friction stir processing. *J Mater Res Technol* 2022; 17: 3150–3156.
13. Jiang L, Huang W, Liu C, et al. Microstructure, texture evolution and mechanical properties of pure Ti by friction stir processing with slow rotation speed. *Mater Charact* 2019; 148: 1–8.
14. Fall A, Monajati H, Khodabandeh A, et al. Local mechanical properties, microstructure, and microtexture in friction stir welded Ti-6Al-4V alloy. *Mater Sci Eng A* 2019; 749: 166–175.
15. Heidarzadeh A, Saeid T, Klemm V, et al. Effect of stacking fault energy on the restoration mechanisms and mechanical properties of friction stir welded copper alloys. *Mater Des* 2019; 162: 185–197.
16. Ebrahimi M and Par MA. Twenty-year uninterrupted endeavor of friction stir processing by focusing on copper and its alloys. *J Alloys Comp* 2019; 781: 1074–1090.
17. Huang G, Wu J, Hou W, et al. Microstructure, mechanical properties and strengthening mechanism of titanium particle reinforced aluminum matrix composites produced by submerged friction stir processing. *Mater Sci Eng A* 2018; 734: 353–363.
18. Chen S, Li X, Jiang X, et al. The effect of microstructure on the mechanical properties of friction stir welded 5A06 Al Alloy. *Mater Sci Eng A* 2018; 735: 382–393.
19. Xie GM, Cui HB, Luo ZA, et al. Asymmetric distribution of microstructure and impact toughness in stir zone during friction stir processed a high strength pipeline steel. *Mater Sci Eng A* 2017; 704: 401–411.
20. Torganchuk V, Vysotskiy I, Malopheyev S, et al. Microstructure evolution and strengthening mechanisms in friction-stir welded TWIP steel. *Mater Sci Eng A* 2019; 746: 248–258.
21. Sato YS, Park SHC, Matsunaga A, et al. Novel production for highly formable Mg alloy plate. *J Mater Sci* 2005; 40: 637–642.
22. Venkateswarlu G, Devaraju D, Davidson MJ, et al. Effect of overlapping ratio on mechanical properties and formability of friction stir processed Mg AZ31B alloy. *Mater Des* 2013; 45: 480–486.
23. Ho Y-H, Man K, Joshi SS, et al. In-vitro biomineralization and biocompatibility of friction stir additively manufactured AZ31B magnesium alloy-hydroxyapatite composites. *Bioact Mater* 2020; 5: 891–901.
24. Sezer N, Evis Z and Koç M. Additive manufacturing of biodegradable magnesium implants and scaffolds: review of the recent advances and research trends. *J Magnes Alloys* 2021; 9: 392–415.
25. Staiger MP, Pietak AM, Huadmai J, et al. Magnesium and its alloys as orthopedic biomaterials: a review. *Biomaterials* 2006; 27: 1728–1734.
26. Qi G, Zhang S, Khor KA, et al. Osteoblastic cell response on magnesium-incorporated apatite coatings. *Appl Surf Sci* 2008; 255: 304–307.
27. Rondanelli M, Faliva MA, Tartara A, et al. An update on magnesium and bone health. *Biometals* 2021; 34: 715–736.
28. Serec K, Babić SD, Podgornik R, et al. Effect of magnesium ions on the structure of DNA thin films: an infrared spectroscopy study. *Nucleic Acids Res* 2016; 44: 8456–8464.
29. Vormann J. Magnesium: Nutrition and homoeostasis. *AIMS Public Health* 2016; 3: 329–340.
30. Tsakiris V, Tardei C and Clicinschi FM. Biodegradable Mg alloys for orthopedic implants – a review. *J Magnes Alloys* 2021; 9: 1884–1905.
31. Agarwal S, Curtin J, Duffy B, et al. Biodegradable magnesium alloys for orthopaedic applications: A review on corrosion, biocompatibility and surface modifications. *Mater Sci Eng: C* 2016; 68: 948–963.
32. Rahim SA, Joseph MA, Sampath Kumar TS, et al. Recent progress in surface modification of Mg alloys for biodegradable orthopedic applications. *Front Mater* 2022; 9: 848980. DOI: 10.3389/fmats.2022.848980.
33. Gzyl M, Rosochowski A, Pesci R, et al. Mechanical properties and microstructure of AZ31B magnesium alloy processed by I-ECAP. *Metallurgical Mater Trans A* 2014; 45: 1609–1620.
34. Kokubo T and Takadama H. How useful is SBF in predicting in vivo bone bioactivity? *Biomaterials* 2006; 27: 2907–2915.
35. Morgan DM. Tetrazolium (MTT) assay for cellular viability and activity. *Methods Mol Biol* 1998; 79: 179–183.
36. Cakmak U, Oz-Tuncay F, Basoglu-Ozdemir S, et al. Synthesis of hydrazine containing piperazine or benzimidazole derivatives and their potential as α-amylase inhibitors by molecular docking, inhibition kinetics and in vitro cytotoxicity activity studies. *Med Chem Res* 2021; 30: 1886–1904.
37. Haarindraprasad R, Hashim U, Gopinath SC, et al. Low temperature annealed zinc oxide nanostructured thin film-based transducers: characterization for sensing applications. *PLoS One* 2015; 10: e0132755–NaN20.
38. Sekban DM, Aktarer SM, Zhang H, et al. Microstructural and mechanical evolution of a low carbon steel by friction stir processing. *Metallurgical Mater Trans A* 2017; 48: 3869–3879.
39. Pavlina EJ and Van Tyne CJ. Correlation of yield strength and tensile strength with hardness for steels. *J Eng Perf* 2008; 17: 888–893.
40. Mironov S, Onuma T, Sato YS, et al. Tensile behavior of friction-stir welded AZ31 magnesium alloy. *Mater Sci Eng A* 2017; 679: 272–281.

41. Li S, Yang X, Tang W, et al. Effect of friction stir processing on microstructure and work hardening behavior of reduced activation ferritic/martensitic steel. *J Manuf Process* 2019; 37: 220–231.
42. Wang YM and Ma E. Three strategies to achieve uniform tensile deformation in a nanostructured metal. *Acta Mater* 2004; 52: 1699–1709.
43. Woo W, Choo H, Prime MB, et al. Microstructure, texture and residual stress in a friction-stir-processed AZ31B magnesium alloy. *Acta Mater* 2008; 56: 1701–1711.
44. Yasavol N and Ramalho A. Wear properties of friction stir processed AISI D2 tool steel. *Tribol Int* 2015; 91: 177–183.
45. Huang J, Wan S, Wang L, et al. Tribological properties of Si-doped graphite-like amorphous carbon film of PEEK rubbing with different counterparts in SBF medium. *Tribol Lett* 2015; 57: 10–18.
46. Vaira Vignesh R, Padmanaban R and Datta M. Influence of FSP on the microstructure, microhardness, intergranular corrosion susceptibility and wear resistance of AA5083 alloy. *Trib-Mater, Surf and Inter* 2018; 12: 157–169.
47. Yuvaraj N and Aravindan S. Fabrication of Al5083/B4C surface composite by friction stir processing and its tribological characterization. *J Mater Res Technol* 2015; 4: 398–410.
48. Iwaszko J and Kudła K. Microstructure, hardness, and wear resistance of AZ91 magnesium alloy produced by friction stir processing with air-cooling. *Int J Adv Manuc Tech* 2021; 116: 1309–1323.
49. Kim JY, Kim DO and Byeon JW. Strength and corrosion resistance of Al-alloying layer on AZ31B magnesium alloy fabricated in situ by reactive friction stir processing. *Mater Charact* 2021; 174: 111024.
50. Tillmann W, Vogli E and Momeni S. Mechanical and tribological properties of Ti/TiAlN duplex coatings on high and low alloy tool steels. *Vacuum* 2009; 84: 387–392.
51. Sert Y, Küçükömeroğlu T, Asl HG, et al. The effect of Al and Ti transition metals on the wear resistance of ceramic based CrN Coatings; investigation under Ambient Air and vacuum conditions. *J Mat Design Appl* 2022; 236: 455–472.
52. Godet M. The third-body approach: A mechanical view of wear. *Wear* 1984; 100: 437–452.
53. Genez Valencia KD, Posada Pérez VM, Fernández Morales GP, et al. Cytotoxic evaluation and biocompatibility of AZ31B alloy for applications in bone tissue engineering. *Prospectiva* 2016; 14: 7–12.
54. Zhang J, Zhang B, Zhang J, et al. Magnesium promotes the regeneration of the peripheral nerve. *Front Cell Dev Biol* 2021; 9: 717854.
55. Schumacher SA, Toribio RE, Lakritz J, et al. Radio-telemetric assessment of cardiac variables and locomotion with experimentally induced hypermagnesemia in horses using chronically implanted catheters. *Front Vet Sci* 2019; 6: 414.
56. Rajan ST, Das M and Arockiarajan A. Biocompatibility and corrosion evaluation of niobium oxide coated AZ31B alloy for biodegradable implants. *Colloids Surf B Biointerfaces* 2022; 212: 2342.